PAPER

Multi-Grid FDTD Calculation of Electromagnetic Absorption in the Human Head for 5 GHz Band Portable Terminals

Jianqing WANG[†], ***Regular Member***, **Hideaki SEKO**[†], ***Nonmember***, **Osamu FUJIWARA**[†], ***and*** **Toshio NOJIMA**[††], ***Regular Members***

SUMMARY A multi-grid finite-difference time-domain (FDTD) method was applied for numerical dosimetry analysis in the human head for 5 GHz band portable terminals. By applying fine FDTD grids to the volumes in the human head where the highest electromagnetic (EM) absorption occurs and coarse grids to the remaining volumes of the head, the spatial peak specific absorption rate (SAR) assessment was achieved with a less computation memory and time. The accuracy of applying the multi-grid FDTD method to the spatial peak SAR assessment was checked in comparison with the results obtained from the usual uniform-grid method, and then the spatial peak SARs for three typical situations of a person using a 5.2 GHz band portable terminal were calculated in conjunction with an anatomically based human head model.

key words: *multi-grid FDTD, electromagnetic absorption, portable terminal, anatomically realistic head model*

1. Introduction

Future mobile communication systems are required to support multimedia services such as voice, text, picture, and image data. This requires the system at least with a bit rate as high as 20 MHz, and consequently a carrier frequency as high as several gigahertz. To this end, the new generation of mobile communication systems is being worldwide investigated at 5 GHz band [1]. The corresponding portable terminals will be used in a great variety of situations such as a laptop computer with a wireless modem. Because users generally hold the portable terminal next to their head in use, it is important to consider the possible health hazards due to the exposure of electromagnetic (EM) fields from the portable terminal antenna at such a high frequency band. The basic exposure limits for these EM hazards are specified in terms of the specific absorption rate (SAR), or the absorbed power in unit mass of tissue. In the USA and Europe, the SAR limits for portable communication devices are specified up to 6 GHz [2] and 10 GHz [3], respectively, whereas in Japan the SAR limits are only specified below 3 GHz [4].

Manuscript received July 10, 2000.
Manuscript revised February 19, 2001.

[†]The authors are with the Department of Electrical and Computer Engineering, Nagoya Institute of Technology, Nagoya-shi, 466-8555 Japan.
[††]The author is with NTT DoCoMo Inc., Yokosuka-shi, 239-8536 Japan.

A possible choice for the guidelines applicable to the portable terminals at 5 GHz band is the power density because the skin depth of human head is as small as 4 mm. Even so it is still necessary to assess the SAR in the human head in order to establish a relationship between the EM absorption in the tissue and the power density.

The most popular simulation technique for assessing the SAR in human head is the finite-difference time-domain (FDTD) method together with an anatomically based human head model [5]–[9]. In the FDTD simulation, a common practice is to divide the geometry of the portable terminal and human head with an FDTD cell size corresponding to at least 10 cells per minimum wavelength for obtaining a reliable result. To satisfy the above condition at 5 GHz band, however, it requires a maximum FDTD cell with a size of about 0.7 mm. This would yield an impractical computer memory requirement because increasing the resolution by n in a 3-dimensional FDTD simulation will increase the memory requirement by n^3 and the computation time by n^4. Gandhi and Chen previously calculated the EM absorption in the human head at such a high frequency band (6 GHz) by using the FDTD method [10]. However, the FDTD cell size employed in their calculation was as large as 1/4 wavelength in tissue. Its accuracy was only verified for the plane-wave exposure.

In order to solve the above-mentioned problem, a multi-grid FDTD method is applied to the spatial peak SAR assessment in the human head. In the multi-grid FDTD, two regions consisting of the coarse main-grid region and fine local-grid region are created. The coarse main-grids are used to model the entire structure, and the fine local-grids, corresponding to at least 10 cells per minimum wavelength, are used to model the portable terminal and the volume in the head where the highest EM absorption occurs. Such an arrangement is based on the fact that the skin depth is very small at 5 GHz band so that the EM fields will only penetrate into the superficial tissue. This makes it possible to obtain a satisfactory simulation result in a reasonable computation memory and time. The accuracy of applying the multi-grid FDTD method to the spatial peak SAR assessment is checked by using the results with usual

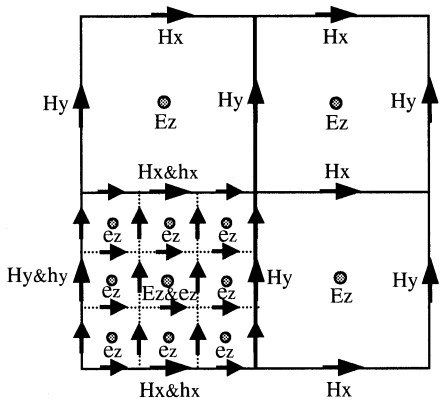

Fig. 1 A main-grid/local-grid structure illustrating the collocated field components.

uniform-grids, and then the spatial peak SARs in conjunction with an anatomically based human head model are given at 5.2 GHz for three situations.

2. Multi-Grid FDTD Method

The multi-grid FDTD method used in this study was introduced by Chevalier et al. in [11]. In the multi-grid FDTD, a coarser main-grid region is created to contain the entire portable-terminal/human-head structure and a finer local-grid region is created to surround the volumes of the portable terminal and human head of interest. Figure 1 shows a main-grid/local-grid structure illustrating the collocated field components. The cells are assumed to be cubical for simplicity and the cell size ratio between the main and local grids is set to an odd integer 3. In such a way every main-grid field value on the main-grid/local-grid (MG-LG) boundary or within the local-grid region has a corresponding local-grid field that is spatially collocated with it. It should be noted that since the magnetic fields, both normal and tangential components, are continuous over the MG-LG boundary for non-magnetic biological tissues, the interpolation scheme used on the MG-LG boundary is largely simplified. Moreover, this arrangement as shown in Fig. 1 is also convenient to define the tissue properties in the local-grid cells.

3. Validity Test

Using the approach described above, we have developed a multi-grid FDTD code for the SAR calculation. Its performance was examined in comparison with full local-grid FDTD results. Figure 2(a) shows the structure used for the validation test, which consists of a 5.2 GHz half-wavelength dipole antenna and a dielectric cube with dimensions of $8 \times 8 \times 8$ cm. The dielectric properties of the cube had the same values as the averages of the brain tissue at 5.2 GHz, i.e., relative permittivity $\varepsilon_r = 39.05$, conductivity $\sigma = 3.66$ S/m, and mass density $\rho = 1030$ kg/m^3 [12]. The SAR distributions in

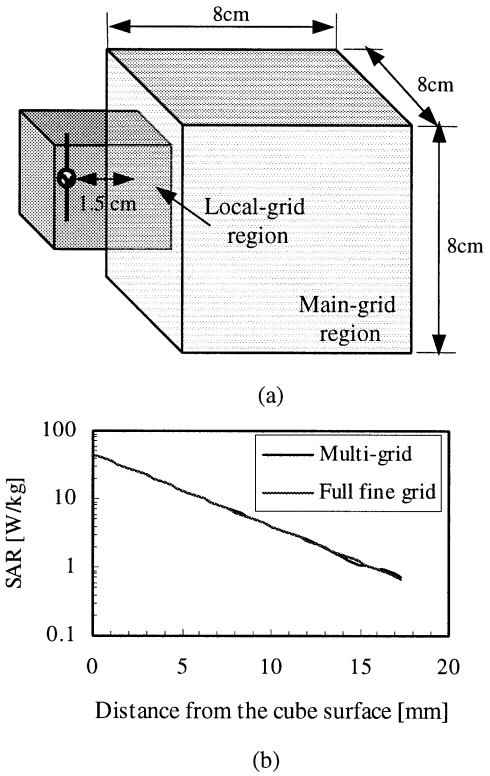

Fig. 2 (a) Geometry of a half-wavelength dipole antenna and a dielectric cube used for the validation test; (b) SAR distributions along a horizontal line through the antenna feed point.

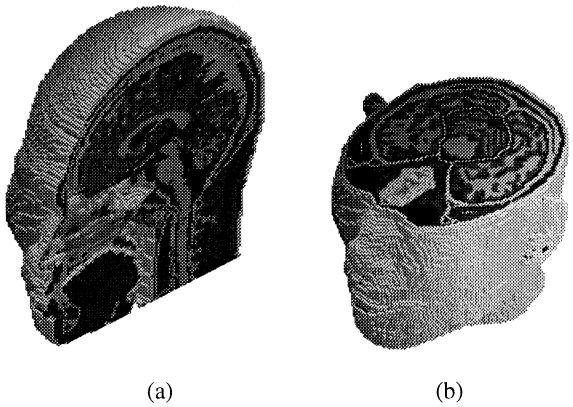

Fig. 3 MRI-based human head model. (a) Mid-sagittal viertical cross-section; (b) horizontal cross-section through the eyes.

the dielectric cube were calculated for the three cases: (1) multi-grid, (2) full fine grid, and (3) full coarse grid. In the multi-grid case, as shown in Fig. 3(a), the dipole antenna and a portion of the dielectric cube, where the highest EM absorption should occur, were divided into 2/3 mm local-grid cells and the rest was divided into main-grid cells with a cell size of 2 mm. In the full fine-grid case, the entire geometry was divided into fine-grid cells with a cell size of 2/3 mm smaller than 1/10 of the minimum wavelength, while in the full coarse-grid case, the entire geometry was divided into coarse-grid cells

Table 1 SAR comparisons for the three test cases.

Test case	Peak SAR [W/kg]	One-gram peak SAR [W/kg]	Local-grid region average SAR [W/kg]	Input impedance [Ω]
Multi-grid	44.75	16.52	3.86	104.87 + j58.38 *
Full fine grid	44.81	16.48	3.86	106.76 + j59.43
Full coarse grid	36.87	13.71	3.06	137.96 + j95.14

Antenna output = 1 W.

* The antenna input impedance was calculated as 78.29+j43.58 Ω when the dielectric cube was removed.

with a cell size of 2 mm. In all of the three cases the dipole antenna had a length of 28 mm, i.e., 42 cells in the multi-grid case or full fine-grid case, and 14 cells in the full coarse-grid case. In addition, the antenna element was modeled by setting the electric field components along the antenna axis to zero, and the antenna excitation was made at the center-cell of the antenna element by the so-called delta gap feeding with a sinusoidal voltage source whose amplitude is V. It is known that such an antenna model corresponds to an antenna with an effective radius δ/e^2 (δ: cell size). Thus the simulated antenna radius was 0.09 mm both in the multi-grid and the full fine-grid cases. To model a dipole antenna with the same radius of 0.09 mm in the full coarse-grid case, the sub-cell method which was applied not only for the antenna element cells but also the feeding gap cell, as described in [16], was employed. Twelve perfectly-matched-layers (PML) [13] were employed as the absorbing boundary conditions to absorb outgoing scattered waves. The calculations for all of the three cases were done for more than 10 cycles (700 main-grid time steps or 2100 local-grid time steps) to obtain a steady-state result. The SAR in each cell was calculated in the steady-state from

$$SAR = \frac{\sigma}{2\rho}|E|^2 \tag{1}$$

and normalized to 1 W antenna output where the antenna output power was defined as

$$P_{out} = \frac{1}{2}Re\,(VI^*) \tag{2}$$

in which I is the complex amplitude of the current obtained from the magnetic fields circling the voltage source according to Ampere's law, and $*$ denotes complex conjugate.

Figure 2(b) shows the SAR distributions along a horizontal line through the antenna feed point, and Table 1 gives the one-gram and ten-gram averaged spatial peak SARs as well as the antenna input impedance. As can be seen, the multi-grid solutions were in excellent agreement with the full fine-grid solutions, which gives confidence to our developed multi-grid FDTD code. However, the full coarse-grid solutions gave underestimated SAR values up to 20% in comparison with the full fine-grid solutions. A major reason for the poor accuracy of coarse-grid solutions attributes to the too large cell size in simulating the EM interaction between the dipole antenna and the head. The poor modeling for the interaction can also be observed from the calculated antenna impedances in Table 1. These results suggest that the coarse-grids can not give a reasonable solution for the near-field exposure at 5.2 GHz.

Table 2 Run time and memory for the two test cases.

Test case	Run time [Min.]	Memory requirement [MByte]
Multi-grid	27	101
Full fine grid	364	557

The run time and memory requirements on a 500 MHz Pentium III personal computer are given in Table 2. Both the run time and required memory for the multi-grid test case were greatly below those of the fine grid. With increasing the volume of geometry for analysis, e.g., for an antenna/human-head structure, the fine grid should provide more efficiency in saving the computation time and memory requirement.

4. Human Head Model

With the multi-grid FDTD method, we calculated the spatial peak SAR in an anatomically based human head model. Figure 3 shows a mid-sagittal vertical cross-section and a horizontal cross-section through the eyes of the human head model. The head model was developed based on magnetic resonance imaging (MRI) data [14]. The original raw MRI data were taken from a Japanese adult head (male, 23 years old), which consists of 115 slices with 2 mm space in the axial plane. Each MRI slice had a 256 × 256 pixel and 9-bit grey scale image. Under the guidance of a medical doctor, the grey scale images were segmented unambiguously as belonging to one of 17 different tissue types by assigning each 2 mm cube voxel to a RGB code, which identifies the discrete tissue type of that particular voxel. Table 3 shows the electrical properties [12] for each tissue.

For applying the multi-grid FDTD method to the 5.2 GHz SAR calculation, each 2 mm cell of the human head within the fine-grid region was re-divided into 27 (3 × 3 × 3) cells. Each of the 27 cells was assigned to the same tissue type as the previous 2 mm cell. Although such a division did not increase the resolution of the human head model (i.e., still being 2 mm), the calculated SARs would have excluded, at least, the numerical errors due to inadequate cell sizes larger than 1/10 of the minimum wavelength.

Table 3 Dielectric properties of tissue at 5.2 GHz.

Tissue	ρ [kg/m^3]	ε_r	σ [S/m]
blood	1060.0	53.60	5.67
bone	1850.0	12.91	1.45
bone marrow	1030.0	8.97	1.02
cartilage	1100.0	33.25	4.29
cornea	1050.0	47.43	4.95
CSF	1010.0	61.59	6.90
dura	1030.0	38.61	3.76
eye humour	1010.0	65.56	5.71
fat	920.0	5.01	0.25
grey matter	1030.0	44.86	4.32
lens	1100.0	36.27	3.35
mucous membrane	1010.0	39.36	3.76
muscle	1040.0	49.85	4.47
parotid gland	1050.0	53.20	5.14
sclera	1170.0	48.70	4.73
skin	1010.0	35.61	3.22
white matter	1030.0	33.24	3.01

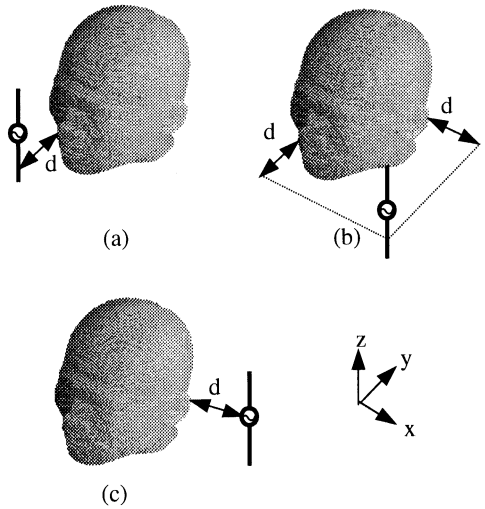

Fig. 4 Geometry of a half-wavelength dipole antenna and the human head model. (a) The antenna is placed in the front of the head; (b) the antenna is placed in the side-front of the head; (c) the antenna is placed in the side of the head. In Figs. (a) and (b), the feed point of the antenna is placed at the same height as the center of the eyeballs. In Fig. (c), the feed point of the antenna is placed at the same height as the center of the auditory canal.

5. Results and Discussion

The spatial peak SAR in the human head was evaluated for three configurations of the antenna as shown in Fig. 4. Figure 4(a) illustrates a geometry of an antenna in the front of the human head (named as front situation), which may be considered as a situation of a top-mounted antenna in a laptop computer or a wireless LAN (local area network) modem. Figure 4(b) illustrates a geometry of an antenna in the side-front of the human head (named as side-front situation), which may be considered as a situation of a side-mounted antenna in a laptop computer or a wireless LAN modem. Figure 4(c) illustrates a geometry of an antenna at the side of the head by the ear (named as side situation), which simulates a situation as a voice phone. In all of the three situations, the antenna was simplified as a half-wavelength dipole at 5.2 GHz and had a vertical alignment. In the front situation, the feed point of the half-wavelength dipole was placed at the same height as the center of the eyeballs with a separation of d from the tip of the nose, while in the side situation, the feed point of the half-wavelength dipole was placed at the almost same height as the center of the auditory canal also with a separation of d from the outer surface of the ear. In the side-front situation, the feed point of the half-wavelength dipole was placed at the same height as the center of the eyeballs, but the dipole was located at the cross-point for the horizontal line along the x-axis with a separation of d from the tip of the nose and the horizontal line along the y-axis also with a separation of d from the ear.

In order to investigate the effect of local-grid region size in the multi-grid FDTD for the human head dosimetry, the local-grid region was first varied from $6 \times 6 \times 6$ cm to $12 \times 12 \times 12$ cm in the front situation. Table 4 gives the size effect on the one-gram and ten-gram averaged spatial peak SARs, in which the one-gram and ten-gram averaged spatial peak SARs were obtained by shifting a cube of $1 \times 1 \times 1$ cm ($1\,\text{cm}^3$) and a cube of $2.2 \times 2.2 \times 2.2$ cm ($10.6\,\text{cm}^3$) across the head volume and by computing $\sigma|E|^2/2\rho$ averaged over the cubes at every position, respectively. No air cells were contained in the cubes. From Table 4, a local-

Table 4 Effect of size of local-grid region on the spatial peak SAR.

Peak SAR	$6 \times 6 \times 6$ [cm]	$8 \times 8 \times 8$ [cm]	$10 \times 10 \times 10$ [cm]	$12 \times 12 \times 12$ [cm]
One-gram peak SAR [W/kg]	3.18	4.02	4.03	4.03
Ten-gram peak SAR [W/kg]	-	-	0.51	0.51

Antenna output = 1 W.
- impossible to obtain a ten-gram averaged spatial peak SAR in a shape of cubic.

Table 5 Effect of the MG-LG boundary on the spatial peak SAR.

Peak SAR	2 main-grid cell far from the antenna	3 main-grid cell far from the antenna	4 main-grid cell far from the antenna
One-gram peak SAR [W/kg]	3.59	4.03	4.03
Ten-gram peak SAR [W/kg]	0.46	0.51	0.51

Antenna output = 1 W.

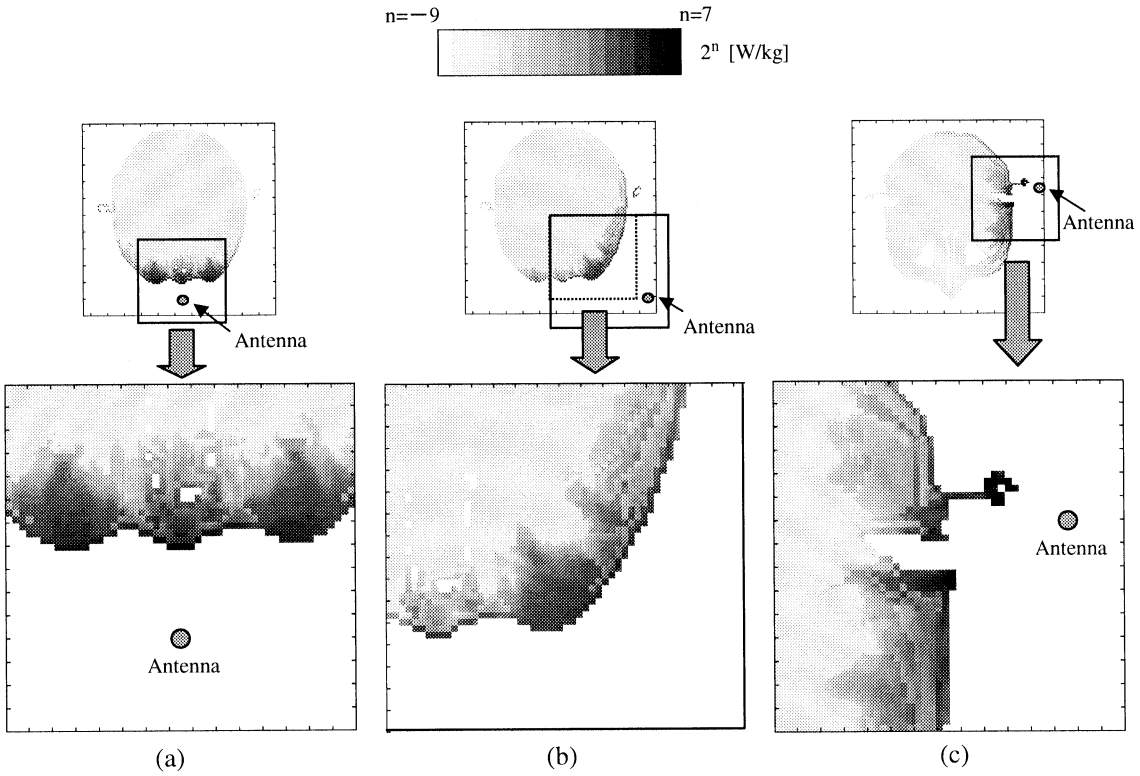

Fig. 5 SAR distribution obtained in the local-grid regions. (a) Front situation; (b) side-front situation (only the SAR values in the dotted-line region are plotted); and (c) side situation. The distance d between the antenna and the head surface is 5 cm.

grid region of $10 \times 10 \times 10$ cm seems to be sufficient to obtain a reliable spatial peak SAR by using the multi-grid FDTD method. The same investigations were also made in the side-front situation and side situation, and the conclusion was not changed.

In addition, a remarkable thing is that, to suppress the reflection by the MG-LG boundary, the factor β [11] for linearly weighting the main-grid and local-grid electric fields closest to the MG-LG boundary was chosen as 0.8 in this study. Our numerical investigations suggested that β was insensitive to the one-gram and ten-gram averaged peak SAR values. For example, changing β between 0.7 to 0.9 only resulted in a variation within 0.02% on the one-gram or ten-gram averaged peak SAR. Another remarkable thing is that the MG-LG boundary should be kept at a distance at least 3 main-grid cell far from the antenna in order not to be affected by the reflection on the MG-LG boundary. Table 5 gives the effect of the MG-LG boundary on the spatial peak SAR, which was also investigated in the front situation with $\beta = 0.8$. When the distance between the MG-LG boundary and the antenna was as close as 2 main-grid cells, an evidently increased antenna input impedance was observed, and consequently an inaccurate SAR value was yielded.

Figure 5 shows the SAR distributions obtained from the local-grid data in the three situations. Also shown in the above figure are the whole head region distributions illustrated with the main-grid data. In each situation the SAR distribution was given in a horizontal cross-section through the antenna feed point, and the separation d was 1.5 cm from the head. As can be seen from Fig. 5, the maximum EM absorption occurred in the region which was closest to the antenna. The EM waves penetrated only the superficial tissue and decreased rapidly with deepening into the head. A strong EM wave approach along the auditory canal was not observed in the side situation. Table 6 summarizes the one-gram and ten-gram averaged spatial peak SARs in the head with various different separation d. A

Table 6 Calculated one-gram and ten-gram averaged spatial peak SARs.

Peak SAR	Separation [cm]	Antenna situation Front	Side-front	Side
One-gram peak SAR [W/kg]	1.5	4.03	1.17	6.61
	3.0	2.62	0.83	3.93
	5.0	1.76	0.51	2.13
Ten-gram peak SAR [W/kg]	1.5	0.51	0.28	0.98
	3.0	0.36	0.20	0.62
	5.0	0.27	0.13	0.35

Antenna output = 1 W.

remarkable phenomenon is that the one-gram averaged spatial peak SAR is much larger than the ten-gram averaged spatial peak SAR. As can be seen, the one-gram averaged spatial peak SAR reached up to 6.61 W/kg for an antenna output of 1 W, while the ten-gram averaged spatial peak SAR dramatically decreased to only 0.98 W/kg in the side situation with a separation of 1.5 cm. In order to identify the reason for such a dramatic difference, the maximum SAR locations in the one-gram average and ten-gram average cubes were investigated. In the front situation, both of the cubes for obtaining the one-gram and ten-gram averaged peak SARs were located in the eyeball region. The maximum SAR value in the the one-gram cube was observed in the eyeball surface (cornea), while the maximum SAR value in the ten-gram cube was observed in the eye humour with a depth of 4 mm from the eyeball surface. However, in the side-front situation or the side situation, the maximum SAR values in the one-gram cube and the ten-gram cube were observed in the same location. The maximum SAR value was observed in the corner of the eye in the side-front situation, and in the front of the ear in the side situation. Both of them were located in the superficial tissue. These facts implies that the dramatic difference between the one-gram and ten-gram averaged SARs is mainly due to the high concentration of EM absorption in the superficial tissue. The ten-gram averaged spatial peak SAR is unlikely to be a proper index for the dosimetry evaluation at 5 GHz band because it cannot reflect the highly concentrated EM absorption in the superficial tissue[†].

Although the concentration of the EM absorption in the superficial tissue releases the concern for possible effects on the brain, it raises another concern about eyes. When the antenna was placed in the front or side-front of the head, some stronger SAR values were observed in the eye region. However, even for the extremely close separation of 1.5 cm, the observed one-voxel peak SARs in the eye were 17.05 W/kg for the front situation and 7.66 W/kg for the side-front situation both with an antenna output of 1 W. The corresponding one-gram averaged peak SARs in the eye were 1.17 W/kg and 0.94 W/kg, respectively. In [15] Hirata et al. have reported a calculated temperature-rise of 0.26°C with respect to a one-gram averaged peak SAR of 3 W/kg in the eye for a plane-wave exposure at 5.8 GHz. Considering that (1) our calculation was made at the similar frequency band and (2) the one-gram averaged peak SAR was smaller than 40% of 3 W/kg, although it was a near-field exposure, we conclude that the resultant maximum temperature-rise in the eye is unlikely to have a possibility of exceeding 0.3°C in any situations with an antenna output of 1 W.

6. Conclusion

A multi-grid FDTD method has successfully been applied to the numerical dosimetry in human head for 5 GHz band portable terminals. Its validity has been examined in comparison with the usual uniform-grid FDTD results. Good agreement has been obtained and an effective saving on computation time and memory has been achieved. By using the multi-grid FDTD method, the spatial peak SARs in three situations of a person using a portable terminal have been calculated in conjunction with an anatomically based human head model at 5.2 GHz. The results have shown that the EM waves at this frequency band penetrates only the superficial tissue and decreases rapidly with deepening into the head. This finding has released the concern for possible effects on the brain, while it raises another concern about eyes. For an extremely close separation of 1.5 cm when the antenna is placed in the front or side-front of the head, the one-gram averaged SAR in the eye would never exceed 1.17 W/kg for an antenna output of 1 W. Referring to the result in [15] for a plane-wave exposure at the similar frequency band, this SAR level is unlikely to cause a temperature rise exceeding 0.3°C in the eye.

Moreover, the finding also implies that the ten-gram averaged spatial peak SAR is not a proper index for the dosimetry evaluation at 5 GHz band. In comparison with the ten-gram averaged peak SAR, the one-gram averaged peak SAR seems to be more reasonable to reflect the highly concentrated EM absorption in such a high frequency band. In addition, due to the very short wavelength, the electromagnetic interaction between the antenna and the human body should be

[†]It should be noted that, for portable terminals, there is not an exposure limit at 5 GHz band in Japan. The Japanese basic safety guidelines, which is generally applied to plane-wave exposure, require that the spatial peak SAR averaged over any one-gram of tissue does not exceed 8 W/kg.

similar to the plane-wave exposure so that the power density may become a useful index for EM absorption assessment.

The further subjects would include the following respects: (1) an elucidation of the relationship between the power density and the spatial peak SAR at this frequency band; (2) a detailed study in the human eyes including the development of high-resolution eye model as well as temperature-rise calculation; and (3) modeling of the portable terminals.

References

[1] T. Kobayashi, M. Umehira, and S. Aikawa, "Goal of broadband wireless access systems—Situation and R&D Activity," Proc. 1998 Commun. Society Conf. of IEICE, PB-2-1.
[2] American National Standards Institute, "Safety levels with respect to exposure to radio frequency electromagnetic fields, 3 kHz to 300 GHz," ANSI/IEEE C95.1-1992.
[3] International Commission on Non-Ionizing Radiation Protection, "ICNIRP statement—Health issues related to the use of hand-held radiotelephones and base transmitters," Health Physics, vol.70, no.4, pp.587–593, April 1996.
[4] Report of Telecommunications Technology Council for the Ministry of Posts and Telecommunications, Deliberation no.89, "Radio-radiation protection guidelines for human exposure to electromagnetic fields," Tokyo, 1997.
[5] P.J. Dimbylow and S.M. Mann, "SAR calculations in an anatomically realistic model of the head for mobile communication transceivers at 900 MHz and 1.8 GHz," Phys. Med. Biol., vol.39, pp.1537–1553, 1994.
[6] M. Okoniewski and M.A. Stuchly, "A study of the handset antenna and human body interaction," IEEE Trans. Microwave Theory & Tech., vol.44, no.10, pp.1855–1864, Oct. 1996.
[7] O.P. Gandhi, G. Lazzi, and C.M. Furse, "Electromagnetic absorption in the human head and neck for mobile telephones at 835 and 1900 MHz," IEEE Trans. Microwave Theory & Tech., vol.44, no.10, pp.1884–1896, Oct. 1996.
[8] S. Watanabe, M. Taki, T. Nojima, and O. Fujiwara, "Characteristics of the SAR distributions in a head exposed to electromagnetic fields radiated by a hand-held portable radio," IEEE Trans. Microwave Theory & Tech., vol.44, no.10, pp.1874–1883, Oct. 1996.
[9] J. Wang and O. Fujiwara, "FDTD computation of temperature rise in the human head for portable telephones," IEEE Trans. Microwave Theory & Tech., vol.47, no.8, pp.1528–1534, Aug. 1999.
[10] O.P. Gandhi and J.Y. Chen, "Electromagnetic absorption in the human head from experimental 6-GHz handheld transceivers," IEEE Trans. Electromagn. Compat., vol.37, no.4, pp.547–558, Nov. 1995.
[11] M.W. Chevalier, R.J. Luebbers, and V.P. Cable, "FDTD local grid with material traverse," IEEE Trans. Antennas & Propag., vol.45, no.3, pp.411–421, March 1997.
[12] C. Gabriel, "Compilation of the dielectric properties of body tissues at RF and microwave frequencies," Brooks Air Force Technical Report AL/OE-TR-1996-0037, 1996.
[13] J.-P. Berenger, "A perfectly matched layer for the absorption of electromagnetic waves," J. Comp. Phys., vol.114, pp.185–200, 1994.
[14] J. Wang and O. Fujiwara, "FDTD analysis of dosimetry in human head model for a helical antenna portable telephone," IEICE Trans. Commun., vol.E83-B, no.3, pp.549–554, March 2000.
[15] A. Hirata, G. Ushio, and S. Shiozawa, "Calculation of temperature rises in the human eye exposed to EM waves in the ISM frequency bands," IEICE Trans. Commun., vol.E83-B, no.3, pp.541–548, March 2000.
[16] S. Watanabe and M. Taki, "An improved FDTD model for the feeding gap of a thin-wire antenna," IEEE Microwave Guided Wave Lett., vol.8, pp.152–154, April 1998.

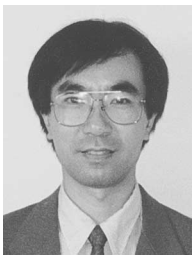

Jianqing Wang received the B.E. degree in electronic engineering from Beijing Institute of Technology, Beijing, China, in 1984, and the M.E. and D.E. degrees in electrical and communication engineering from Tohoku University, Sendai, Japan, in 1988 and 1991, respectively. He was a Research Associate at Tohoku University and a Research Engineer at Sophia Systems Co., Ltd., prior to joining the Department of Electrical and Computer Engineering, Nagoya Institute of Technology, Nagoya, Japan, in 1997, where he is currently an Assistant Professor. His research interests include electromagnetic compatibility, bioelectromagnetics and digital communications.

Hideaki Seko received the B.E. degree in electrical and computer engineering from Nagoya Institute of Technology, Nagoya, Japan, in 2000. He is currently engaged in the study on computational electromagnetics towards the M.E. degree.

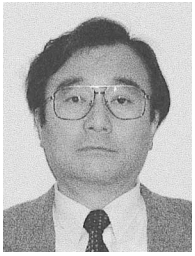

Osamu Fujiwara received the B.E. degree in electronic engineering from Nagoya Institute of Technology, Nagoya, Japan, in 1971, and the M.E. and the D.E. degrees in electrical engineering from Nagoya University, Nagoya, Japan, in 1973 and in 1980, respectively. From 1973 to 1976, he worked in the Central Research Laboratory, Hitachi, Ltd., Kokubunji, Japan, where he was engaged in research and development of system packaging designs for computers. From 1980 to 1984 he was with the Department of Electrical Engineering at Nagoya University. In 1984 he moved to the Department of Electrical and Computer Engineering at Nagoya Institute of Technology, where he is presently a professor. His research interests include measurement and control of electromagnetic interference due to discharge, bioelectromagnetics and other related areas of electromagnetic compatibility. Dr. Fujiwara is a member of the IEE of Japan and of the IEEE.

Toshio Nojima received the B.E. degree in electrical engineering from Saitama University, Japan, in 1972, and the M.E. and Ph.D. degrees in electronic engineering from Hokkaido University, Japan, in 1974 and 1988, respectively. From 1974 to 1992, he was with the Nippon Telegraph and Telephone (NTT) Communications Laboratories, where he was engaged in the development of high capacity 6-GHz SSB-AM and 256-QAM systems. Following these, he has been working for the development of highly efficient radio circuit technologies including super conducting devices for cellular radio systems. Since 1992, he has been with the NTT DoCoMo Inc., Yokosuka, where he is currently a Senior Executive Research Engineer. His research fields also cover EMC studies including RF safety issues. He is a member of the IEEE.